

Mixed-Valence Single-Atom Catalyst Derived from Functionalized Graphene

Aristides Bakandritsos, Ravishankar G. Kadam, Pawan Kumar, Giorgio Zoppellaro, Miroslav Medved', Jiří Tuček, Tiziano Montini, Ondřej Tomanec, Pavlína Andrýšková, Bohuslav Drahoš, Rajender S. Varma, Michal Otyepka, Manoj B. Gawande,* Paolo Fornasiero,* and Radek Zbořil*


Single-atom catalysts (SACs) aim at bridging the gap between homogeneous and heterogeneous catalysis. The challenge is the development of materials with ligands enabling coordination of metal atoms in different valence states, and preventing leaching or nanoparticle formation. Graphene functionalized with nitrile groups (cyanographene) is herein employed for the robust coordination of Cu(II) ions, which are partially reduced to Cu(I) due to graphene-induced charge transfer. Inspired by nature's selection of Cu(I) in enzymes for oxygen activation, this 2D mixed-valence SAC performs flawlessly in two O₂-mediated reactions: the oxidative coupling of amines and the oxidation of benzylic C–H bonds toward high-value pharmaceutical synthons. High conversions (up to 98%), selectivities (up to 99%), and recyclability are attained with very low metal loadings in the reaction. The synergistic effect of Cu(II) and Cu(I) is the essential part in the reaction mechanism. The developed strategy opens the door to a broad portfolio of other SACs via their coordination to various functional groups of graphene, as demonstrated by successful entrapment of Fe^{III}/Fe^{II} single atoms to carboxy-graphene.

Heterogeneous nanocatalysis based on metallic species has undoubtedly evolved into a central discipline because it offers solutions to meet the challenges in the field.^[1] Restricting the dimensions of the catalytically active particles down to few nanometers^[2] or even to subnanometer clusters,^[3,4] has proven pivotal for enhancing performance. Flytzani-Stephanopoulos and co-workers in 2003^[5] highlighted the activity of supported Au and Pt single metal ions in water gas shift catalysts, while following reports^[6–10] shed more light on single-atom catalysts

(SACs) (see also reviews^[11–13]). SACs could offer ultimate atom economy and make every active site accessible, like homogeneous catalysts but being recyclable, which is a subject of paramount importance.^[14] Major challenges in the field though encompass: i) the development of materials with precise functionalities for robust metal ion binding and ii) metal cooperativity in heterometallic and mixed-valence SACs, as identified in the recent topical perspective.^[12] Meeting the first challenge could facilitate higher metal contents avoiding clustering and leaching upon reaction and catalyst recycling. This is also a prerequisite for the second challenge (metal–metal cooperation), since low metal content translates into large intermetallic distances.^[6] Cooperation between two metal ions linked by a single-frame ligand has shown enormous potential in homogeneous catalysis.^[15] For example, biocatalysts (metalloenzymes) use binuclear^[16] and mixed-valence metal centers^[17] for effective catalysis. Therefore, the development of heterogeneous catalysts with cooperativity between metal centers, keeping all the salient features of SACs, could offer a platform for the development of the next generation of catalysts.

Graphene-based 2D materials have contributed to the development of SACs,^[10,12–14,18–27] in which metal ions are tetraordinated in porphyrinic-like vacancies. Although only low contents of metal atoms can be achieved (up to ≈1 wt%),^[10,12,14,18,22–26]

Dr. A. Bakandritsos, Dr. R. G. Kadam, Dr. P. Kumar, Dr. G. Zoppellaro, Dr. M. Medved', Dr. J. Tuček, O. Tomanec, P. Andrýšková, Dr. R. S. Varma, Prof. M. Otyepka, Dr. M. B. Gawande, Prof. R. Zbořil
Regional Centre of Advanced Technologies and Materials
Department of Physical Chemistry
Faculty of Science
Palacký University Olomouc
Šlechtitelů 27, 783 71 Olomouc, Czech Republic
E-mail: manoj.gawande@upol.cz; radek.zboril@upol.cz

 The ORCID identification number(s) for the author(s) of this article can be found under <https://doi.org/10.1002/adma.201900323>.

Prof. P. Fornasiero, Prof. T. Montini
Department of Chemical and Pharmaceutical Sciences
INSTM Trieste Research Unit and ICCOM-CNR Trieste Research Unit
University of Trieste
via L. Giorgieri 1, I-34127 Trieste, Italy
E-mail: pforasiero@units.it

Dr. B. Drahoš
Regional Centre of Advanced Technologies and Materials
Department of Inorganic Chemistry
Faculty of Science
Palacký University Olomouc
17. listopadu 12, 771 46 Olomouc, Czech Republic

DOI: 10.1002/adma.201900323

nanoparticle formation often persists,^[19–21,27] thus limiting metal–metal cooperation and atom economy. Sintering and nanoparticle formation in these SACs should be probably attributed to the high temperature^[6,14,19,20,27] and high energy (e.g., ball milling^[21]) procedures required for their preparation. For these reasons, installation of functional groups on graphene, which can bind metal ions through typical coordination chemistry methods, would lift such limitations.

In the present work, we designed a mixed-valence ionic copper catalyst delivering exceptional conversions and selectivities (see Table S1, Supporting Information) with very low metal loading in the reaction, for the oxidative homo-/hetero-dehydrogenation of amines to imines and benzylic C–H bond oxidation, through which a wide variety of pharmaceutically important compounds are commercially produced.^[28,29] The catalyst was prepared on multi-gram scale exploiting the abundant cyano-functionalities of a previously developed graphene derivative (cyanographene, G-CN),^[30] as strong and selective ligands for copper ions.^[31] The bare G–CN support was synthesized by our previously reported method^[30] via substitution of fluorine atoms in fluorographene with nitrile groups. Subsequently, G–CN was mixed with CuCl₂ to immobilize Cu(II) on the G–CN sheets (Figure 1a). The binding of copper was verified with inductively coupled plasma mass spectrometry (ICP-MS), amounting to ≈3.4 wt%. High-resolution transmission electron microscopy (HR-TEM, Figure 1b) and X-ray diffraction (Figure S1, Supporting Information) verified the absence of inorganic crystalline phases, and in the former case unveiled high electron density spots, ascribed to copper ions before (Figure 1c,d) and after the catalytic reaction (Figure 1e,f). The Cu single atoms were also identified with scanning transmission electron microscopy (STEM, Figure S2, Supporting Information). The spot size of the Cu atoms is ≈0.2 nm, in accordance with experimental results and simulations on copper phthalocyanine over graphene.^[32] Chemical mapping revealed the homogeneous distribution of Cu over the graphene (Figure 1g,h). Definitive proof on the single-atom state of copper and information about their coordination environment were collected by electron paramagnetic spectroscopy (EPR) measurements, as discussed later, and X-ray absorption spectroscopy (Figure S3, Supporting Information).

High-resolution X-ray photoelectron spectroscopy (HR-XPS) revealed reduction of ≈50% of the Cu(II) ions to Cu(I). The Cu 2p envelope (Figure 1i) indicated two valence states: Cu(I) at 932.6 eV and Cu(II) at 934.9 eV, with areas of 55% and 45%, respectively. The completely different HR-XPS of a control sample with graphene oxide (Figure S4, Supporting Information) supported the hypothesis that the presence of Cu(I) ions should be attributed to interactions developed specifically with G–CN. EPR and X-ray absorption near edge structure also verified the presence of Cu(I) and that it is not the result of reduction from the XPS beam (Figures S3 and S5, Supporting Information). In order to explain the reduction, we used density functional theory (DFT) calculations, which showed that the positive charge and spin density on copper significantly decreased, and that charge transfer indeed facilitates the reduction of Cu(II) to Cu(I) (Figure 1j–l; Table S2, Supporting Information). Analysis of the HR-XPS N1s envelope experimentally corroborated the charge transfer and the interaction between

the N-atom from G–CN and Cu cations, as explained in Figure S6 in the Supporting Information.

The mixed-valence Cu SAC was employed for the oxidative homo-/hetero-dehydrogenation of amines to imines (Figure 2a and b) and benzylic C–H bond oxidation (Figure 2c), through which a wide variety of pharmaceutically important compounds are commercially produced.^[28,29] Once the reaction conditions for amine-homocoupling were optimized (Table S3, Supporting Information), the catalyst delivered very high selectivities and no undesirable byproducts for a large variety of amines (except for 2-picolyamine, Figure 2(g), with negligible amounts of aldehyde and amides). For amines substituted with electron withdrawing groups, such as the para-chloro-derivative (Figure 2(c)), the catalyst showed excellent conversion and selectivity despite the fact that such substrates generally lead to lower conversions (i.e., 77.5%, 393 K with an MnO_x/CeO₂ catalyst^[33]). For the strongly electron withdrawing CF₃-substituted benzylamine (Figure 2(e)), G(CN)–Cu displayed higher turnover frequency (TOF = 13 h^{–1}) at lower temperatures than the currently best-performing nanoparticulate catalysts (CuO nanoflakes^[34] or mesoporous Cs/MnO_x^[35] with TOF ≈3 h^{–1}). For the S-substituted derivative, G(CN)–Cu showed superior performance (Figure 2(j)), even with respect to homogeneous catalysts.^[36] Homocoupling of alkylamines is particularly sluggish due to the presence of the inactive α-hydrogen.^[37] It is very remarkable that the G(CN)–Cu catalyst achieved comparatively high conversion for this challenging reaction (Figure 2(k)).

The versatility of the catalyst was also investigated for the heterocoupling of substituted benzylic amines with anilines (Figure 2b). Heterocoupling with high selectivity is not straightforward, as it competes with self-coupling. Nevertheless, after optimization of the molar ratio of amines to anilines (Table S4, Supporting Information), excellent conversion and selectivities were achieved (Figure 2b). For example, cross-coupling reaction between benzyl amine with aniline leads to a very poor selectivity, 23% with CuCl₃^[38] versus 95% with G(CN)–Cu. The potency of the catalyst is further unveiled by considering the results obtained from a cesium-doped mesoporous manganese oxide catalyst, reported to promote cross-coupling very effectively with solvent and under air^[35] (selectivities 10–70%, but only 15% conversion for benzylamine–aniline coupling). In the present case over 99% selectivity was obtained for benzylamine–aniline coupling under solvent-free conditions and lower temperature (Figure 2(5a)). Metal-free, graphene-like systems have also been reported for catalytic cross-coupling of amines, but generally they require extremely high catalyst loadings (50%),^[39] even in the case of photocatalytically active carbon nitride catalysts.^[40] In general, the performance of G(CN)–Cu appears to be superior in comparison to state-of-the-art catalysts, as demonstrated in detail in Table S1 in the Supporting Information.

Inspired by the excellent results on oxidative amine coupling, the catalyst was further challenged for the selective benzylic C–H oxidation of hydrocarbon derivatives (Figure 2c). Selective oxidation of saturated C–H bonds is one of the most important protocols in fine chemical synthesis and industrial chemistry due to the wide applications of oxidized products in the agricultural and pharmaceutical sectors.^[29] The reactions were studied under oxygen and mild conditions. Notably, although such reactions were previously performed under high

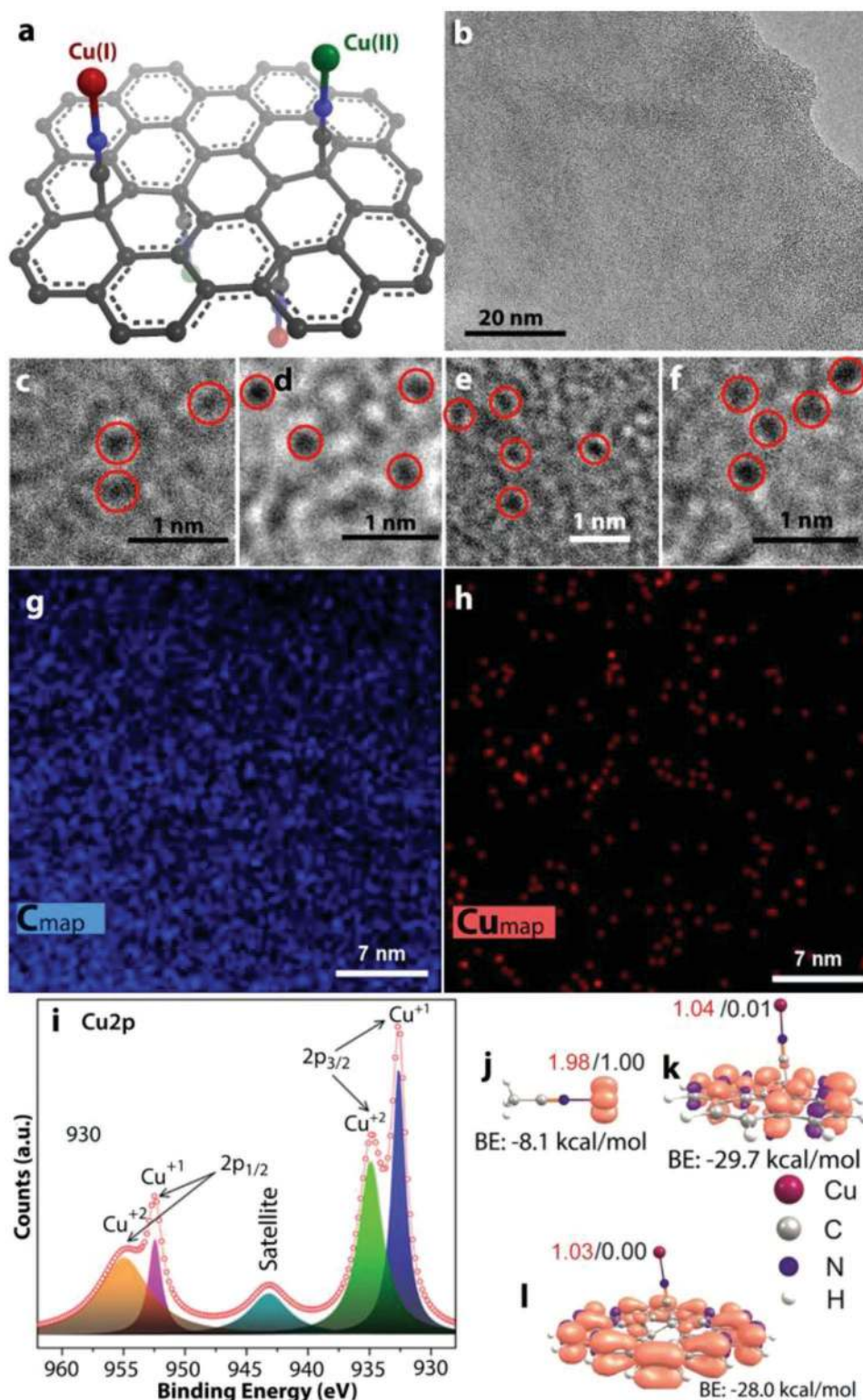


Figure 1. a) Model of the mixed-valence copper catalyst. b) Representative HR-TEM of a graphene flake from the G(CN)—Cu catalyst. c–f) Representative higher magnification HR-TEM images from the catalyst showing high-contrast spots originating from embedded copper atoms c,d) before and e,f) after the catalytic reaction. EDS chemical mapping of G(CN)—Cu for g) C and h) Cu. i) HR-XPS on Cu2p of the G(CN)—Cu catalyst. j–l) Natural charge (red text), spin density plots (colored surfaces), and spin density values on Cu ions (black text), as well as binding energies (BE) regarding Cu(II) in R—CN...Cu(II) model systems in their doublet state: j) Acetonitrile...Cu(II); k) Coronene-2CN...Cu(II); and l) Cyc14-2CN...Cu(II) (circumprylene, system with 14 aromatic cycles and two nitrile groups) computed at the SMD/B3LYP/6-31+G(d) level of theory. In (j) Cu ion is not visible due to the spin density plot overlap.

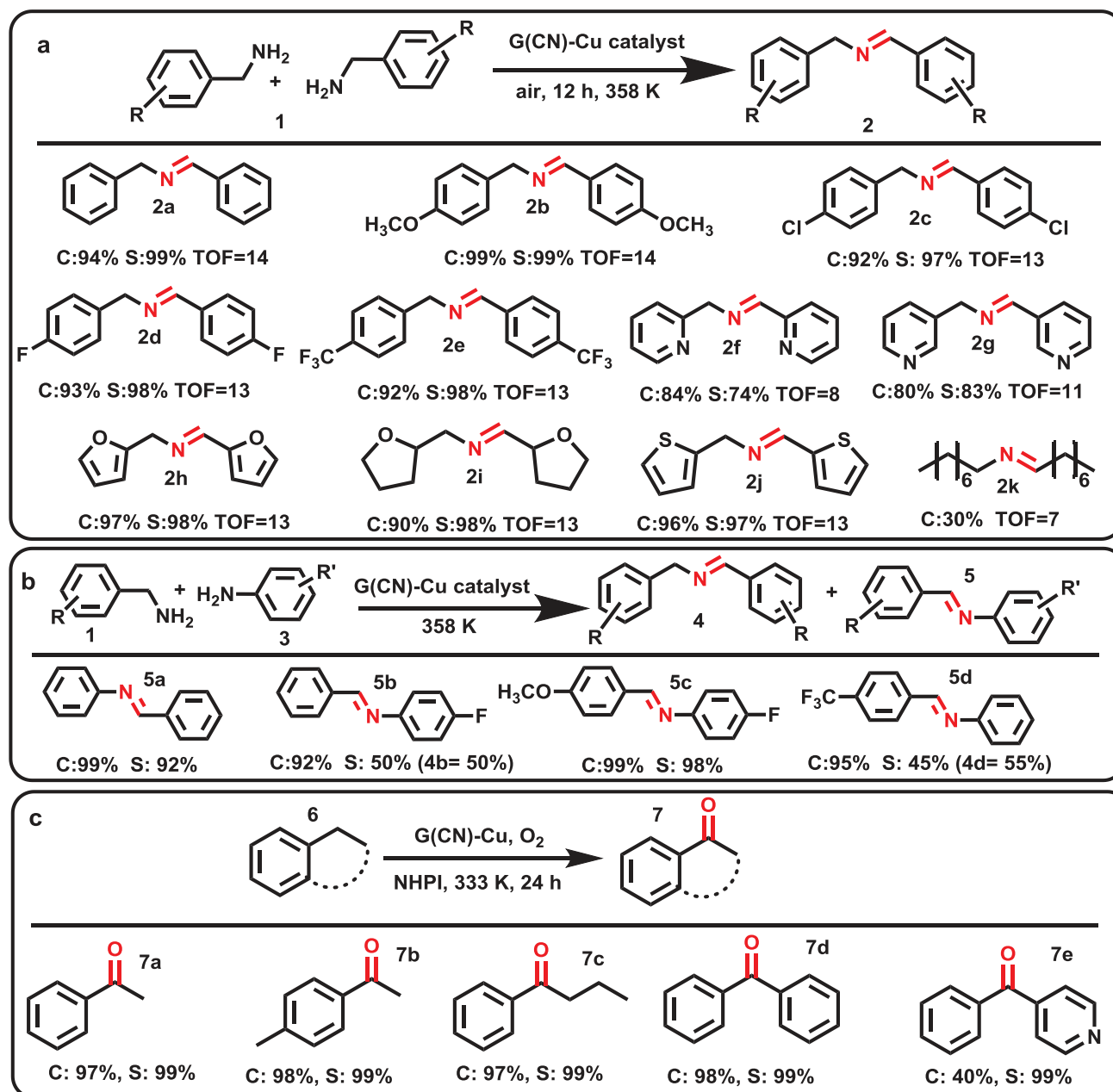


Figure 2. a) Oxidative homocoupling of substituted benzylamines. Reaction conditions: 20 mg of the G(CN)–Cu catalyst or 10.7 μmol of Cu (i.e., 0.58 mol% Cu reaction loading), 1.83 mmol of amine substrate, 358 K, 12 h, air balloon (1 atm); TOF given in h^{-1} . Reaction time 24 h for product 2k. b) Oxidative cross-coupling of benzylamines with anilines. Reaction conditions: amines 1.83 mmol, aniline 5.49 mmol (amines:aniline molar ratio 1:3), 24–30 h. Catalyst and other conditions same as in (a). c) Oxidation reactions of benzylic C–H bonds. Reaction conditions: ethylbenzene (0.5 mmol), *N*-hydroxyphthalimide (NHPI) 15 mol%, 10 mg of G(CN)–Cu (5.3 $\mu\text{mol}_{\text{Cu}}$) in 3 mL of acetonitrile under O_2 (1 atm). In all reactions the G(CN)–Cu catalyst was used; conversions (C) and selectivities (S) were determined by gas chromatography.

oxygen pressure (10 bar),^[41] using noble metals ($\text{ReOCl}_3(\text{OPPh}_3)$ (SMe_2),^[42] and/or high temperature (120 °C), poor conversions/selectivities (36–75%) were attained.^[41,43] However, the present catalyst yielded good to excellent conversions (up to 98%) and selectivities (up to 99%) under mild conditions (Figure 2c).

Importantly, the catalyst revealed very high stability upon recycling, remaining highly active (94% conversion; same as the fresh one, see Figure 2(2a), product 2a) for benzylamine

coupling, even after five recycling steps (Figure 3a). Moreover, no change in product selectivity was detected and thus *N*-benzylidene-benzylamine was synthesized with 98% selectivity during all catalytic cycles. XPS analysis after the reaction, verified that the copper mixed-valence state was retained (Figure 3b; Figure S7 and Table S5, Supporting Information). Post-recycling HR-TEM analysis and energy-dispersive X-ray spectroscopy (EDS) chemical mapping also

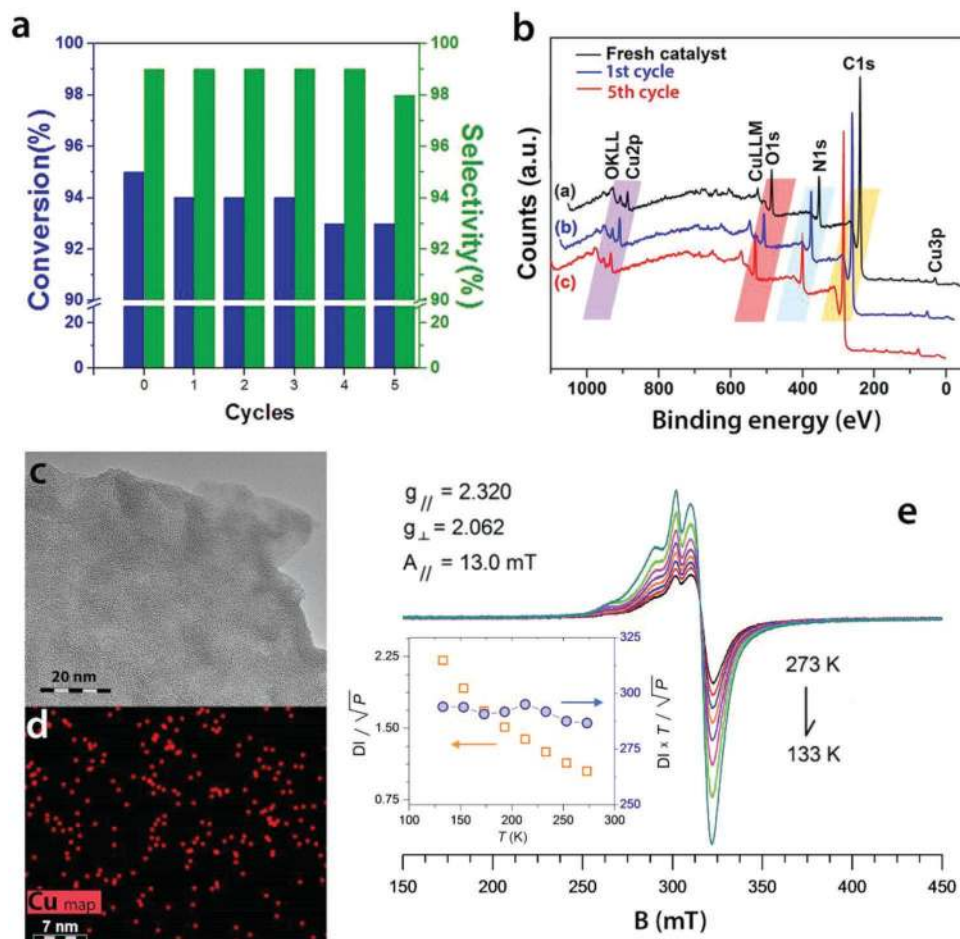


Figure 3. a) Recycling experiments using the G(CN)–Cu catalyst for oxidative coupling of benzylamine. b) XPS spectra of the G(CN)–Cu catalyst (a) before reaction, (b) after the 1st recycling, and (c) after the 5th recycling. c) HR-TEM image of the catalyst after five catalytic cycles showing absence of nanoparticles. d) EDS copper mapping on the catalyst after five catalytic reactions. e) X-band (9.156588 GHz) powder spectra of G(CN)–Cu catalyst recorded inside a polypropylene VSN holder (P125E) in the temperature range of 273–133 K. Experimental parameters: 100 kHz modulation frequency, 30 ms time constant, 4 min sweep time, 0.4 mW microwave power, 0.7 mT modulation width. The inset shows the temperature (T) dependence of the EPR signal, expressed either as double-integrated signal intensity divided by the square root of the applied microwave power (DI/\sqrt{P} , circles) or as $DI \times T/\sqrt{P}$ (squares).

confirmed the absence of any inorganic nanoparticles after the 5th catalytic cycle (Figure 3c,d) and that the Cu ion distribution was just as homogeneous as in the fresh catalyst.

The single-atom character of the catalyst and the absence of any Cu(0) or CuO nanoparticles were also demonstrated clearly by low-temperature EPR measurements (Figure 3e). The EPR spectrum of the fresh catalyst exhibits a broad resonance signal that is fully consistent with the presence of isolated paramagnetic Cu(II) cations (d^9 system). It should be noted that the presence of Cu(I) cations (d^{10} system) cannot be confirmed by EPR, since Cu(I) is silent. The unpaired electron in Cu(II) ($S = 1/2$) is clearly localized in the d orbital ($g_{\text{eff}} > 2.0023$) and experiences a moderate tetragonal ligand-field ($g_{\parallel} > g_{\perp}$). DFT calculations also supported the tetragonal coordination environment as the most stable one, with binding energy of $-27.1 \text{ kcal mol}^{-1}$ (Table S6, Supporting Information). At this point, it is very difficult to resolve the exact coordination environment of the as-prepared and freeze-dried catalyst, i.e., how many water molecules Cu atoms might

be coordinated with. Only the $\Delta m_s = 1$ transition is detected (around $g = 2$); no half-field transition (around $g = 4$, $\Delta m_s = 2$) is observed, suggesting that the effective dipolar interactions (which give rise to the zero-field-splitting (ZFS) term) between copper centers in the system are very weak.^[44–46] The biquadratic ZFS comprises a first-order term, arising from direct spin–spin interaction between magnetic dipoles, and a second-order contribution arising from spin–orbit coupling. Because the direct spin–spin interaction exhibits $1/r^3$ dependence on the ZFS, where r is the distance between magnetically interacting centres, the through-space distances of Cu(II) sites ($S = 1/2$) in G(CN)–Cu must be rather large ($>0.7 \text{ nm}$). The observed Curie behavior ($DI = C/T$) (inset in Figure 3e), further excludes the presence of magnetically interacting Cu(II) centers in the catalyst. That is to say, it excludes the presence of Cu(II) centers that are exchange-coupled through space via Cu–O–Cu bonds, and also the formation of CuO nanoparticles/clusters, which should exhibit antiferromagnetic interactions.^[47]

Although the main scope of this work was the design and characterization of a new class of SACs, we also addressed a probable mechanism via DFT calculations and EPR spectroscopy, in order to explain the superior performance of the catalyst. We focused on one of the reactions (oxidative amine coupling), since both are based on oxygen-activation mediated by the metal and oxidation by hydrogen abstraction (Figure 4a; Figure S9, Supporting Information), which

are typically performed in nature by α -hydroxylating mono-oxygenases^[29] (non-coupled binuclear Cu enzymes^[17]). Following DFT data, benzylamine ligands lead to more stable G(CN)-Cu complexes, than in the case of water molecules (see Tables S6–S8, Supporting Information), thus initiating the reaction (Figure 4a, step 1). The oxidative dehydrogenation of the amine can proceed through reduction of oxygen, as widely accepted.^[28] With knowledge in hand about oxygen reduction

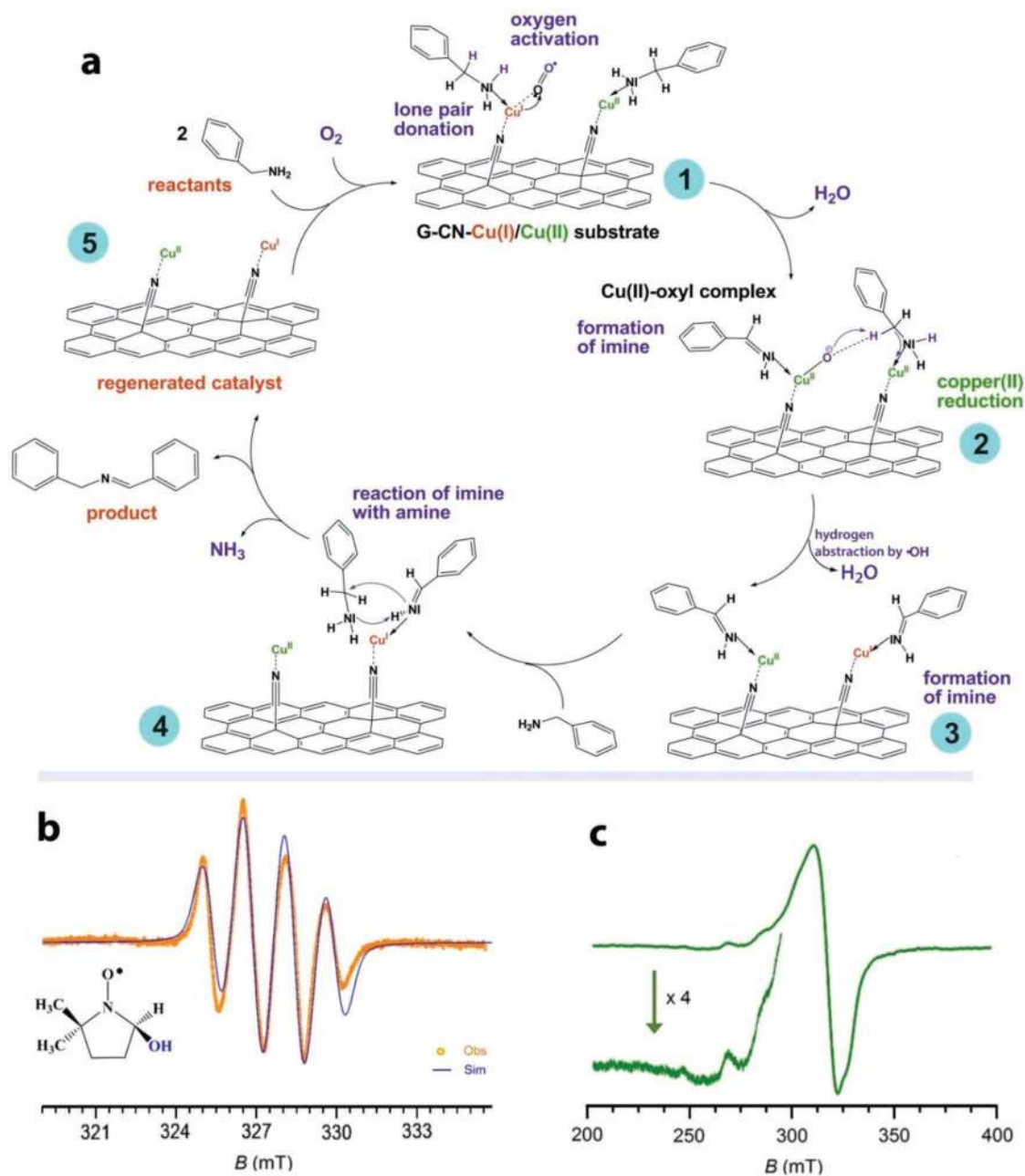


Figure 4. a) The potential main steps of the catalytic reaction (details are available in Figures S8–S12, Supporting Information). b) Identification of the $\cdot\text{OH}$ radicals formed during the catalytic reaction. X-band (9.17 GHz) EPR spectrum of the DMPO–OH radical adduct in solution as obtained after collecting the supernatant by centrifugation of the reaction mixture (catalyst/benzylamine) where the radical trapping agent was added (DMPO/ CH_2Cl_2) (Obs). The blue spectrum (Sim) represents the simulated EPR envelope (see the Supporting Information for details). c) X-band EPR spectrum of the G(CN)–Cu catalyst after turnover. Experimental parameters: frequency 9.1706 GHz, mod. freq. 100 kHz, mod. amplitude of 1.0 mT, time const. of 30 ms, applied microwave power of 0.6 mW, sweep time of 240 s, phase 0° , $T = 123$ K.

in copper enzymes through its preferential coordination with Cu(I) centers,^[16,17,48,49] the Cu(I) center in our catalyst can also play a key role for O₂ binding and activation (Figure 4a, step 1 and Figure S8, steps 1-I, 2-I, Supporting Information) leading to the copper-oxyl intermediate (Figure 4a, step 2 and Figure S8, step 3-I, Supporting Information). A cyclic intermediate can be formed between two Cu ions (Figure 4a, step 2 and Figure S8, step 3-I, Supporting Information), which promotes a two-hydrogen abstraction from the neighboring amine by the reactive oxyl species (Figure S9, Supporting Information) leading to the release of water and formation of an imine molecule (Figure 4a, step 3). Importantly, hydroxyl radicals evolving in this step were trapped and observed by EPR using 5,5-dimethyl-1-pyrroline-*N*-oxide (DMPO) (Figure 4b). Finally, the catalytic cycle could be completed by the amine–imine coupling (Figure 4a, step 4; Figure S10, Supporting Information), leading to the release of NH₃ and to the regeneration of the catalyst (Figure 4a, step 5; Figure S11, Supporting Information).

The cooperativity of Cu ions (through the cyclic intermediate) was also supported experimentally by the powder EPR spectrum of the catalyst, which showed increasing dipolar interactions between Cu centers only after the catalytic reaction (Figure 4c). Since Cu(I) is silent in EPR, the spectrum is dominated by a Cu(II) signal expressing the following spin-Hamiltonian parameters: g_{\parallel} of 2.360 and g_{\perp} of 2.066 and resolved A_{\parallel} of 19 mT. However, a second minor component could be seen (enlarged, low-field spectrum in Figure 4c), which indicated increased rhombic strain probably due to the bond flipping with estimated spin-Hamiltonian parameters: g_1 of 2.380, g_2 of 2.075, and g_3 of 2.005, and with $A_{\parallel} \approx 9.5$ mT. Namely, Cu(II) hyperfine term that is half of that witnessed for the dominant Cu(II) EPR signal. This minor component suggests the presence of weakly interacting copper (II) ions through space ($S_{1,2} = 1/2-1/2$) at distances smaller than 7 Å, where the exchange energy (J) is larger than the Cu hyperfine term (A), i.e., $J > 0.009$ cm⁻¹. This cooperativity is not precluded based on the 7 Å maximum mean distance between the Cu ions, as calculated from the Cu content in G(CN)–Cu (3.4 wt%) and from the experimentally determined surface area (153 m² g⁻¹) of G(CN)–Cu (Table S9, Supporting Information). Further strong evidence for Cu(I)/Cu(II) cooperativity in the G(CN)–Cu catalyst was collected by performing additional control experiments involving the heterocoupling of benzylamine and aniline (Table S10, Supporting Information). Reactions catalyzed by Cu(I) and Cu(II) chlorides, individually or as mixtures, exhibited low conversions (47–60%) and no selectivity (0–8%) for the cross-coupled product. The low activity of the non-immobilized Cu(I)/Cu(II) salt mixtures can be attributed to the inability of freely moving metal ions to stabilize a cyclic intermediate. A catalyst with much less copper (≈ 0.5 wt% instead of 3.4 wt%, and thus with decreased areal density of Cu atoms and limited cooperativity) was also tested in the same reaction. (Table S10, entry 4 in the Supporting Information). To avoid reducing the quantity of copper available for catalysis, the total quantity of this G(CN)–Cu(0.5) catalyst added to the reaction mixture was 7 times that of the G(CN)–Cu(3.4) catalyst used originally. Nevertheless, the selectivity for the desired cross-coupled product fell from 92% to 38%. This can be explained by the increased distance between adjacent Cu(I)/Cu(II) atoms in the low Cu

catalyst, and the resulting reduction in cooperativity. Because aniline lacks α -hydrogens, it cannot undergo hydrogen abstraction and activation, without forming a cyclic intermediate (see Figure S13 in the Supporting Information and the associated mechanistic discussion). These control experiments clearly demonstrate the importance of having immobilized Cu ions in close proximity to one another. Therefore, the higher activity of the densely populated G(CN)–Cu catalyst can be only connected to cooperativity effects.

Overall, the conductive character of G–CN, which mediated the charge transfer for the partial reduction of Cu(II) to Cu(I) ions, leads to excellent catalytic activity of newly developed mixed-valence SAC in comparison to other state-of-the-art catalysts. According to the previously suggested mechanism, this behavior could be attributed to: i) the copresence of Cu(I) promotes binding and activation of oxygen, kick-starting the reaction, ii) neighboring Cu(I)/Cu(II) species are relevant for cyclic intermediate formation and securing the redox balance in the reactions taking place concomitantly at the two copper centers and, finally, iii) the single-atom and under-coordinated state of the metal centers are crucial for furnishing this reaction effectively at low reaction loadings and provide sterically unhindered access for balanced binding and release of reactants, intermediates, and products.

Finally, the possibility to generalize the concept of mixed-valence 2D SACs immobilized on graphene derivatives was demonstrated by the Fe(III)/(II) single atom entrapment (using Fe(NO₃)₃·9H₂O as iron source) on a carboxylated graphene derivative (i.e., graphene acid, which was recently reported and synthesized after the acidic hydrolysis of G–CN^[30]). This Fe/graphene derivative (G(COOH)–Fe) was prepared via a similar procedure as for G(CN)–Cu (see the Supporting Information). Single Fe atoms were identified in HR-TEM/EDS images without any indices of nanoparticles (Figure S14, Supporting Information). The mixed valence state was clearly unveiled by low temperature ⁵⁷Fe Mössbauer spectroscopy (both Fe(III) and Fe(II) species were identified, Figure S15 and Table S11, Supporting Information), suggesting partial charge transfer from graphene to Fe³⁺ centers, as in the case of the G(CN)–Cu catalyst.

We believe this work paves the way for a yet unexplored field of 2D coordination chemistry with covalent graphene derivatives containing suitable donor groups including thiols,^[50] carboxyls,^[30] or hydroxyls.^[51] This concept stimulates the vision of a broad family of single-atom heterogeneous catalysts based on the selective coordination by functional groups of various metals (e.g., Au, Fe, Ni, Co, Pt, Mn) with superior ability to create mixed-valence or bimetallic single-metal-ion catalysts tailored for particular catalytic reactions.

Supporting Information

Supporting Information is available from the Wiley Online Library or from the author.

Acknowledgements

The authors acknowledge Jana Stráská (TEM), Petra Bazgerová (TEM), Dr. David Milde (ICP), Martin Petr (XPS) for the measurements,

Miroslav Vavrečka for synthesis of various metal graphene hybrids (including the carboxy-graphene/Fe system), Tomáš Steklý for contributing in synthesis of G-CN, rGO-Cu, and G(CN)-Cu and Dr. Ondřej Malina for the Mössbauer measurements. The authors acknowledge SOLEIL for provision of synchrotron radiation facilities and Dr. Emiliano Fonda for assistance in using beamline SAMBA. The authors gratefully acknowledge support from the Ministry of Education, Youth and Sports of the Czech Republic (project LO1305, CZ.1.05/2.1.00/19.0377, and CZ.02.1.01/0.0/0.0/16_019/0000754), the ERC (Consolidator grant 683024 from the European Union's Horizon 2020 research and innovation programme), the support from the Czech Science Foundation under Project No. 19-27454X, and the assistance provided by the Research Infrastructure NanoEnviCz under project LM2015073. TM and PF acknowledge the University of Trieste (program FRA 2018 – project INSIDE), the Italian Ministry for University and Research (MIUR – program FFARB 2017) and INSTM consortium.

Conflict of Interest

The authors declare no conflict of interest.

Keywords

amine coupling, C–H oxidation, cooperative catalysis, graphene, single-atom catalysis

Received: January 15, 2019

Published online: February 27, 2019

- [1] R. V. Jagadeesh, K. Murugesan, A. S. Alshammari, H. Neumann, M.-M. Pohl, J. Radnik, M. Beller, *Science* **2017**, *358*, 326.
- [2] M. Cargnello, V. V. T. Doan-Nguyen, T. R. Gordon, R. E. Diaz, E. A. Stach, R. J. Gorte, P. Fornasiero, C. B. Murray, *Science* **2013**, *341*, 771.
- [3] E. C. Tyo, S. Vajda, *Nat. Nanotechnol.* **2015**, *10*, 577.
- [4] D. Yang, B. C. Gates, *Nat. Mater.* **2017**, *16*, 703.
- [5] Q. Fu, H. Saltsburg, M. Flytzani-Stephanopoulos, *Science* **2003**, *301*, 935.
- [6] B. Qiao, A. Wang, X. Yang, L. F. Allard, Z. Jiang, Y. Cui, J. Liu, J. Li, T. Zhang, *Nat. Chem.* **2011**, *3*, 634.
- [7] P. Yin, T. Yao, Y. Wu, L. Zheng, Y. Lin, W. Liu, H. Ju, J. Zhu, X. Hong, Z. Deng, G. Zhou, S. Wei, Y. Li, *Angew. Chem., Int. Ed.* **2016**, *55*, 10800.
- [8] L. Nie, D. Mei, H. Xiong, B. Peng, Z. Ren, X. I. P. Hernandez, A. DeLaRiva, M. Wang, M. H. Engelhard, L. Kovarik, A. K. Datye, Y. Wang, *Science* **2017**, *358*, 1419.
- [9] M. Yang, S. Li, Y. Wang, J. A. Herron, Y. Xu, L. F. Allard, S. Lee, J. Huang, M. Mavrikakis, M. Flytzani-Stephanopoulos, *Science* **2014**, *346*, 1498.
- [10] H. Fei, J. Dong, C. Wan, Z. Zhao, X. Xu, Z. Lin, Y. Wang, H. Liu, K. Zang, J. Luo, S. Zhao, W. Hu, W. Yan, I. Shakir, Y. Huang, X. Duan, *Adv. Mater.* **2018**, *30*, 1802146.
- [11] M. Flytzani-Stephanopoulos, B. C. Gates, *Annu. Rev. Chem. Biomol. Eng.* **2012**, *3*, 545.
- [12] J. Liu, *ACS Catal.* **2017**, *7*, 34.
- [13] X. Cui, W. Li, P. Ryabchuk, K. Junge, M. Beller, *Nat. Catal.* **2018**, *1*, 385.
- [14] H. Fei, J. Dong, Y. Feng, C. S. Allen, C. Wan, B. Voloskiy, M. Li, Z. Zhao, Y. Wang, H. Sun, P. An, W. Chen, Z. Guo, C. Lee, D. Chen, I. Shakir, M. Liu, T. Hu, Y. Li, A. I. Kirkland, X. Duan, Y. Huang, *Nat. Catal.* **2018**, *1*, 63.
- [15] S. Sabater, J. A. Mata, E. Peris, *Nat. Commun.* **2013**, *4*, 2553.
- [16] N. Sträter, T. Klabunde, P. Tucker, H. Witzel, B. Krebs, *Science* **1995**, *268*, 1489.
- [17] P. Chen, E. I. Solomon, *J. Am. Chem. Soc.* **2004**, *126*, 4991.
- [18] X.-F. Yang, A. Wang, B. Qiao, J. Li, J. Liu, T. Zhang, *Acc. Chem. Res.* **2013**, *46*, 1740.
- [19] X. Zhang, J. Guo, P. Guan, C. Liu, H. Huang, F. Xue, X. Dong, S. J. Pennycook, M. F. Chisholm, *Nat. Commun.* **2013**, *4*, 1924.
- [20] H. Fei, J. Dong, M. J. Arellano-Jiménez, G. Ye, N. D. Kim, E. L. G. Samuel, Z. Peng, Z. Zhu, F. Qin, J. Bao, M. J. Yacamán, P. M. Ajayan, D. Chen, J. M. Tour, *Nat. Commun.* **2015**, *6*, 8668.
- [21] K. Jiang, S. Siahrostami, A. J. Akey, Y. Li, Z. Lu, J. Lattimer, Y. Hu, C. Stokes, M. Gangishetty, G. Chen, Y. Zhou, W. Hill, W.-B. Cai, D. Bell, K. Chan, J. K. Nørskov, Y. Cui, H. Wang, *Chem* **2017**, *3*, 950.
- [22] H. B. Yang, J. Miao, S.-F. Hung, J. Chen, H. B. Tao, X. Wang, L. Zhang, R. Chen, J. Gao, H. M. Chen, L. Dai, B. Liu, *Sci. Adv.* **2016**, *2*, e1501122.
- [23] M. Li, S. Wu, X. Yang, J. Hu, L. Peng, L. Bai, Q. Huo, J. Guan, *Appl. Catal., A* **2017**, *543*, 61.
- [24] C. Zhang, J. Sha, H. Fei, M. Liu, S. Yazdi, J. Zhang, Q. Zhong, X. Zou, N. Zhao, H. Yu, Z. Jiang, E. Ringe, B. I. Yakobson, J. Dong, D. Chen, J. M. Tour, *ACS Nano* **2017**, *11*, 6930.
- [25] A. Zitolo, N. Ranjbar-Sahraie, T. Mineva, J. Li, Q. Jia, S. Stamatin, G. F. Harrington, S. M. Lyth, P. Krtíl, S. Mukerjee, E. Fonda, F. Jaouen, *Nat. Commun.* **2017**, *8*, 957.
- [26] A. Zitolo, V. Goellner, V. Armel, M.-T. Sougrati, T. Mineva, L. Stievano, E. Fonda, F. Jaouen, *Nat. Mater.* **2015**, *14*, 937.
- [27] Y. Zheng, Y. Jiao, Y. Zhu, Q. Cai, A. Vasileff, L. H. Li, Y. Han, Y. Chen, S.-Z. Qiao, *J. Am. Chem. Soc.* **2017**, *139*, 3336.
- [28] M. T. Schümperli, C. Hammond, I. Hermans, *ACS Catal.* **2012**, *2*, 1108.
- [29] J. Genovino, D. Sames, L. G. Hamann, B. B. Touré, *Angew. Chem., Int. Ed.* **2016**, *55*, 14218.
- [30] A. Bakandritsos, M. Pykal, P. Błorński, P. Jakubec, D. D. Chronopoulos, K. Poláková, V. Georgakilas, K. Čépe, O. Tomanec, V. Ranc, A. B. Bourlinos, R. Zbořil, M. Otyepka, *ACS Nano* **2017**, *11*, 2982.
- [31] R. D. Pike, *Organometallics* **2012**, *31*, 7647.
- [32] A. Mittelberger, C. Kramberger, J. C. Meyer, *Sci. Rep.* **2018**, *8*, 4813.
- [33] P. Sudarsanam, B. Hillary, M. H. Amin, S. B. A. Hamid, S. K. Bhargava, *Appl. Catal., B* **2016**, *185*, 213.
- [34] R. Singuru, Q. T. Trinh, B. Banerjee, B. Govinda Rao, L. Bai, A. Bhaumik, B. M. Reddy, H. Hirao, J. Mondal, *ACS Omega* **2016**, *1*, 1121.
- [35] S. Biswas, B. Dutta, K. Mullick, C.-H. Kuo, A. S. Poyraz, S. L. Suib, *ACS Catal.* **2015**, *5*, 4394.
- [36] S. Zhao, C. Liu, Y. Guo, J.-C. Xiao, Q.-Y. Chen, *J. Org. Chem.* **2014**, *79*, 8926.
- [37] C. Su, M. Acik, K. Takai, J. Lu, S. Hao, Y. Zheng, P. Wu, Q. Bao, T. Enoki, Y. J. Chabal, K. P. Loh, *Nat. Commun.* **2012**, *3*, 1298.
- [38] R. D. Patil, S. Adimurthy, *Adv. Synth. Catal.* **2011**, *353*, 1695.
- [39] H. Huang, J. Huang, Y.-M. Liu, H.-Y. He, Y. Cao, K.-N. Fan, *Green Chem.* **2012**, *14*, 930.
- [40] F. Su, S. C. Mathew, L. Möhlmann, M. Antonietti, X. Wang, S. Blechert, *Angew. Chem., Int. Ed.* **2011**, *50*, 657.
- [41] P. Zhang, H. Lu, Y. Zhou, L. Zhang, Z. Wu, S. Yang, H. Shi, Q. Zhu, Y. Chen, S. Dai, *Nat. Commun.* **2015**, *6*, 8446.
- [42] H. Peng, A. Lin, Y. Zhang, H. Jiang, J. Zhou, Y. Cheng, C. Zhu, H. Hu, *ACS Catal.* **2012**, *2*, 163.
- [43] X. Lin, Z. Nie, L. Zhang, S. Mei, Y. Chen, B. Zhang, R. Zhu, Z. Liu, *Green Chem.* **2017**, *19*, 2164.
- [44] M. Gullotti, L. Santagostini, R. Pagliarin, S. Palavicini, L. Casella, E. Monzani, G. Zoppellaro, *Eur. J. Inorg. Chem.* **2008**, *2008*, 2081.
- [45] F. G. Mutti, G. Zoppellaro, M. Gullotti, L. Santagostini, R. Pagliarin, K. K. Andersson, L. Casella, *Eur. J. Inorg. Chem.* **2009**, *2009*, 554.

- [46] F. G. Mutti, M. Gullotti, L. Casella, L. Santagostini, R. Pagliarin, K. K. Andersson, M. F. Iozzi, G. Zoppellaro, *Dalton Trans.* **2011**, 40, 5436.
- [47] S. S. Eaton, K. M. More, B. M. Sawant, G. R. Eaton, *J. Am. Chem. Soc.* **1983**, 105, 6560.
- [48] A. Bhagi-Damodaran, M. A. Michael, Q. Zhu, J. Reed, B. A. Sandoval, E. N. Mirs, S. Chakraborty, P. Moënne-Loccoz, Y. Zhang, Y. Lu, *Nat. Chem.* **2017**, 9, 257.
- [49] S. T. Prigge, B. A. Eipper, R. E. Mains, L. M. Amzel, *Science* **2004**, 304, 864.
- [50] V. Urbanová, K. Holá, A. B. Bourlinos, K. Čépe, A. Ambrosi, A. H. Loo, M. Pumera, F. Karlický, M. Otyepka, R. Zbořil, *Adv. Mater.* **2015**, 27, 2305.
- [51] J. Tuček, K. Holá, A. B. Bourlinos, P. Błorński, A. Bakandritsos, J. Ugolotti, M. Dubecký, F. Karlický, V. Ranc, K. Čépe, M. Otyepka, R. Zbořil, *Nat. Commun.* **2017**, 8, 14525.